Crystal and magnetic structures of the spin-trimer compounds $Ca_3Cu_{3-x}Ni_x(PO_4)_4$ ($x=0,1,2$)

V. Yu. Pomjakushin, A. Furrer, and D. V. Sheptyakov
Laboratory for Neutron Scattering, ETH Zurich and Paul Scherrer Institut, CH-5232 Villigen PSI, Switzerland

E. V. Pomjakushina
Laboratory for Developments and Methods, PSI, and Laboratory for Neutron Scattering, ETH Zurich and Paul Scherrer Institut, CH-5232 Villigen PSI, Switzerland

K. Conder
Laboratory for Developments and Methods, PSI, CH-5232 Villigen PSI, Switzerland

(Received 22 May 2007; published 21 November 2007)

Crystal and magnetic structures of a series of quantum spin-trimer system $Ca_3Cu_{3-x}Ni_x(PO_4)_4$ ($x=0,1,2$) were studied by neutron powder diffraction at temperatures of 1.5–290 K. The composition with one Ni per trimer ($x=1$) has a monoclinic structure (space group $P2_1/a$, No. 14) with the unit cell parameters $a=17.71$ Å, $b=4.89$ Å, $c=8.85$ Å, and $\beta=123.84°$ at $T=290$ K. The $x=2$ composition crystallizes in the $C2/c$ space group (No. 15) with the doubled unit cell along the c axis. Each trimer is formed by two crystallographic positions: one in the middle and the second one at the ends of the trimer. We have found that the middle position is occupied by the Cu^{2+}, whereas the end positions are equally populated with the Cu^{2+} and Ni^{2+} for $x=1$ while in the $x=2$ the trimers were found to be of only one type Ni-Cu-Ni. Below $T_N=20$ K, the $x=2$ compound shows an antiferromagnetic ordering with propagation vector star $\{[\frac{1}{2},\frac{1}{2},0],[-\frac{1}{2},\frac{1}{2},0]\}$. The magnetic structure is very well described with the irreducible representation τ_2 using both arms of the star $\{\mathbf{k}\}$ with the magnetic moments of 1.89(1) and 0.62(2) μ_B for Ni^{2+} and Cu^{2+} ions, respectively. We note that our powder diffraction data cannot be fitted by a model containing only one arm of the propagation vector star. The Cu/Ni spins form both parallel and antiparallel configurations in the different trimers, implying substantial effect of the intertrimer interaction on the overall magnetic structure.

DOI: 10.1103/PhysRevB.76.174433 PACS number(s): 75.30.Et, 61.12.Ld, 61.66.Fn

I. INTRODUCTION

The low-dimensional magnets have been attracting attention during last years since they show new interesting quantum effects and also because they are considered as a model system to study very complex phenomena, such as high-temperature superconductivity in metal oxides. $A_3Cu_3(PO_4)_4$ ($A=Ca,Sr,Pb$) is a novel quantum spin-trimer system[1] in which the three Cu^{2+} ($S=\frac{1}{2}$) spins are antiferromagnetically coupled giving rise to a doublet ground state, as determined by neutron spectroscopy.[2] The trimer clusters form one-dimensional (1D) chains with weak but not negligible intertrimer interaction[3,4] leading to a long-range magnetic ordering at $T_C=0.91$ K, $T_N=0.91$ K, and $T_N=1.26$ K for $A=Ca$, Sr, and Pb, respectively. By substituting a Cu^{2+} spin in the trimer by Ni^{2+} ($S=1$), a singlet ground state could be, in principle, realized offering the observation of the Bose-Einstein condensation (BEC) in a quantum spin-trimer system similar to the field-induced BEC of the bosonic triplet state in the spin dimer system $TlCuCl_3$ observed by the inelastic neutron scattering.[5] The substitution of Cu by Ni was successfully realized in the $Ca_3Cu_{3-x}Ni_x(PO_4)_4$ ($x=1,2$) resulting in the new mixed trimer phase with the structure parameters close to the ones of the pristine material ($x=0$). The magnetic excitations in this series were studied by the inelastic neutron scattering[6] making use of the structure data reported in the present paper. The observed excitations were associated with transitions between the low-lying electronic states of trimers. The nearest-neighbor exchange interactions within the trimers in the $x=1,2$ compounds were determined to be also antiferromagnetic with $J_{Cu\text{-}Cu}=-4.92(6)$ meV and $J_{Cu\text{-}Ni}=-0.85(10)$ meV and an axial single-ion anisotropy parameter $D_{Ni}=-0.7(1)$ meV. The ground state was found to be doublet, triplet, and quintet in the Cu-Cu-Cu, Cu-Cu-Ni, and Ni-Cu-Ni trimers, respectively, that are the basic con-

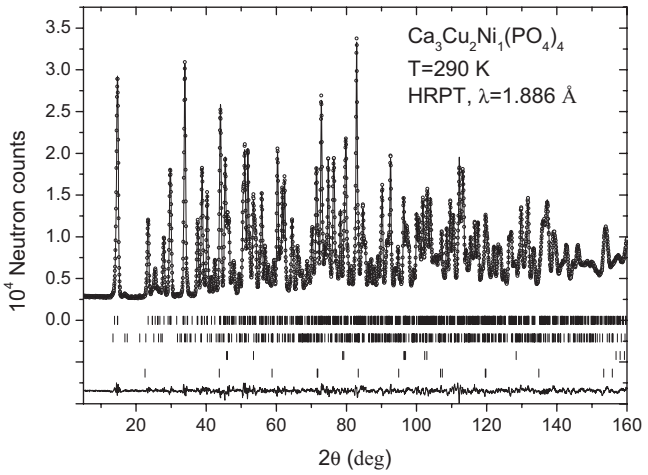

FIG. 1. The Rietveld refinement pattern and difference plot of the neutron diffraction data for the sample $Ca_3Cu_{3-x}Ni_x(PO_4)_4$ ($x=1$) at $T=290$ K measured at HRPT with the wavelength $\lambda=1.886$ Å. The rows of ticks show the Bragg peak positions for the main phase and two impurity phases: whitlockite and NiO nuclear and NiO magnetic peaks (from top to bottom).

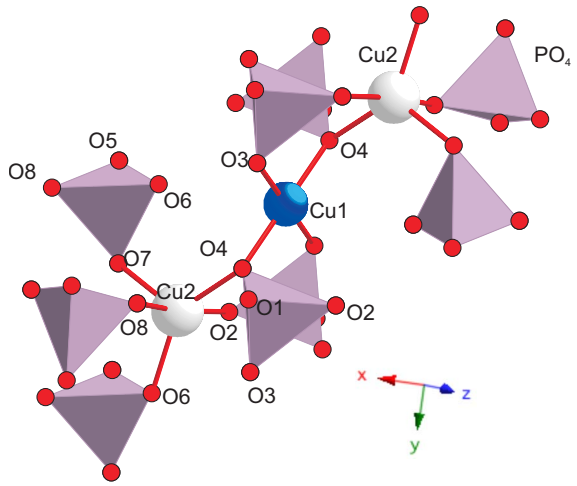

FIG. 2. (Color online) Fragment of the crystal structure showing Cu2-O4-Cu1-O4-Cu2 trimer and the surrounding PO_4 tetrahedra. The positions of the atoms and some selected interatomic distances are listed in Table I.

stituents of the title compounds. The hypothesis of realizing the singlet ground state that motivated the present work was not met, but without the detailed structural information, the analysis of the magnetic excitations could not be performed. In this paper, we present the results of the neutron and synchrotron x-ray powder diffraction study of the crystal and magnetic structures of $Ca_3Cu_{3-x}Ni_x(PO_4)_4$ $(x=0,1,2)$.

II. EXPERIMENT

Polycrystalline samples of $Ca_3Cu_{3-x}Ni_x(PO_4)_4$ $(x=0,1,2)$ were synthesized by a solid state reaction using CuO, NiO, $CaCO_3$, and $NH_4H_2PO_4$ of a minimum purity of 99.99%. The respective amounts of the starting reagents were mixed and heated in alumina crucibles very slowly up to 600 °C and then annealed at 900 °C during at least 100 h, with several intermediate grindings. The ac magnetic susceptibility $\chi(T)=\chi'(T)+i\chi''(T)$ was measured in zero external field with amplitude of the ac field of 10 Oe and frequency

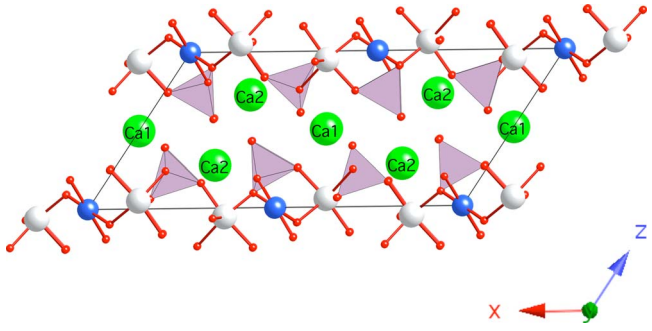

FIG. 3. (Color online) Projection of the crystal structure of $Ca_3Cu_{3-x}Ni_x(PO_4)_4$ on the *ac* plane showing connectivity of the trimers. The Cu1 and Cu2 positions are shown by blue and white balls, the tetrahedra are PO_4, the red sticks indicate Cu-O bonds, and the big green balls are the Ca atoms.

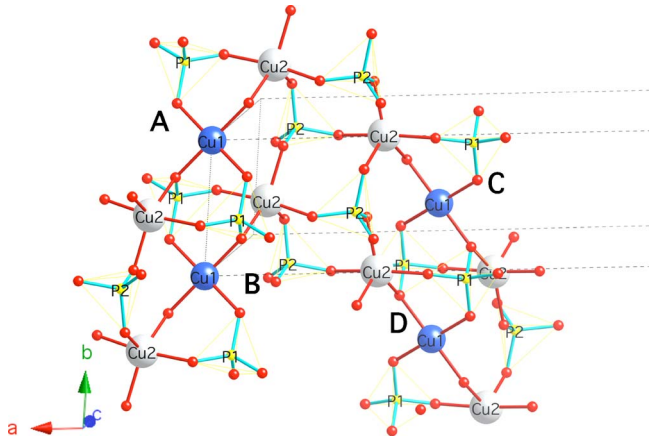

FIG. 4. (Color online) View of four trimers (A, B, C, and D) projected approximately to the *ab* plane in $Ca_3Cu_{3-x}Ni_x(PO_4)_4$ showing possible superexchange paths between the trimers in the *ab* plane. The Cu1 and Cu2 positions are shown by blue and white balls, the tetrahedra with yellow balls in the center are PO_4, the red sticks indicate Cu-O bonds, and the Ca atoms are not shown. Each trimer is formed by the central Cu1 atom and two Cu2 atoms related by inversion with respect to the Cu1 position.

of 1 kHz using Quantum Design PPMS station. Neutron powder diffraction experiments were carried out at the SINQ spallation source of Paul Scherrer Institute (Switzerland) using the high-resolution diffractometer for thermal neutrons HRPT[7] ($\lambda=1.866$ Å, high intensity mode $\Delta d/d \geq 1.8\cdot 10^{-3}$) and the DMC diffractometer[8] situated at a supermirror coated guide for cold neutrons at SINQ ($\lambda=4.2$ Å). All the temperature scans were carried out on heating. *x*-ray synchrotron diffraction measurements at room temperature were done at the Material Sciences beamline (MS, SLS/PSI). The refinements of the crystal and magnetic structure parameters were

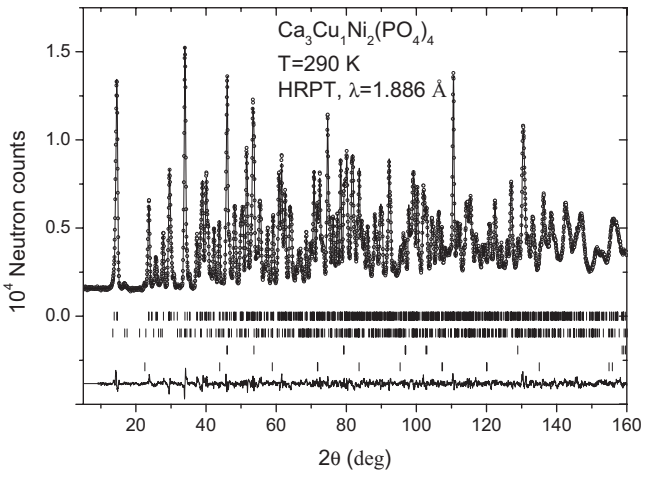

FIG. 5. The Rietveld refinement pattern and difference plot of the neutron diffraction data for the sample $Ca_3Cu_{3-x}Ni_x(PO_4)_4$ $(x=24)$ at $T=290$ K measured at HRPT with the wavelength $\lambda=1.886$ Å. The rows of ticks show the Bragg peak positions for the main phase and two impurity phases.

carried out with FULLPROF program,[9] with the use of its internal tables for scattering lengths and magnetic form factors.

III. CRYSTAL STRUCTURE

Both $x=0$ and $x=1$ compounds have the same space group $P2_1/a$ with the structure parameters shown in Table I. The diffraction pattern and the refinement plot for the $x=1$ sample are shown in Fig. 1. There is a small admixture of two impurity phases: whitlockite $[Ca_{19}Cu_2(PO_4)_{14}]$ and nickel oxide (NiO) that are indicated by the additional rows of ticks. The structure parameters of the whitlockite phase were fixed by the values reported in Ref. 10. The NiO phase has two rows of ticks due to additional antiferromagnetic phase. The mass fractions of the whitlockite and NiO are 2.2(2)%, 0% and 3.3(1)%, 0.20(2)% in the $x=0$ and $x=1$ compositions, respectively. An important block of structure is the Cu2-Cu1-Cu2 trimer that is shown in Fig. 2 together with the surrounding PO_4 tetrahedra. The crystal structure consists of PO_4 tetrahedra connecting the Cu trimers in chains running along the a axis as shown in Fig. 3. Figure 4 shows the view of the trimer connectivity projected roughly to the ab plane.

One can see that the strongest intertrimer interaction is expected to be along the b axis, giving the quasi-1D trimer chains $(\cdots AB\cdots)$ and $(\cdots CD\cdots)$, where A, B, C, and D denote the trimers shown in Fig. 4. There are two superexchange paths between the Cu1(A) and Cu2(B) ions that go through two PO_4 tetrahedra Cu1(A)-O-P1-O-Cu2(B) and also two similar paths between Cu2(A)-Cu1(B) ions. In addition, the distance between the Cu2(A)-Cu1(B) ions is the shortest one ($d_{\mathrm{Cu2(A)\text{-}Cu1(B)}}=3.4$ Å, whereas $d_{\mathrm{Cu1(A)\text{-}Cu1(B)}}=4.9$ Å), providing the largest dipole interaction. The interaction between the 1D chains of trimers along the a axis is mediated by the two superexchange paths between Cu2 ions Cu2(A)-O-P2-O-Cu2(C) as shown in Fig. 4. The intertimer interaction along the c axis (Fig. 3) is the weakest one since the path contains an additional Ca-O link and the ions are separated by a large distance of $d_{\mathrm{Cu2\text{-}Cu2}}=6.5$ Å.

The Ni atom in the $x=1$ sample occupies the Cu2 positions at the ends of the trimers, whereas the middle position Cu1 is occupied by Cu. The end positions are equally populated by both Cu and Ni ions. The occupancy factors can be reliably refined due to significantly different coherent scattering lengths of Ni (10.3 fm) and Cu (7.7 fm) nuclei. The fit model assumed that we have two Cu atoms and one Ni atom per formula unit, allowing them to occupy both Cu1 and Cu2 sites. The refined occupancies are listed in Table I.

The composition with two Ni atoms ($x=2$) crystallizes in a different space group $C2/c$ with a doubled unit cell along the c axis. The transformation from the $P\,1\,2_1/a\,1$ to the $C\,1\,2/c\,1$ structure is given by the matrix $\mathbf{A}=\mathbf{a}$, $\mathbf{B}=\mathbf{b}$, $\mathbf{C}=2\mathbf{c}$ and the origin shift $\mathbf{p}=\mathbf{a}/2$. The structure solution was done with the FOX program[11] using the synchrotron x-ray diffraction pattern collected at the wavelength $\lambda=0.9185$ Å. Final refinement of the neutron diffraction data resulted in the structure parameters listed in Table I. The experimental and the refined diffraction patterns are shown in Fig. 5. In spite of the doubled unit cell, the density of the Bragg peaks is the same as for the $x=0,1$ compositions due to C-centered Bravais lattice. The mass fractions of the whitlockite and NiO impurities amounted to 6.4(2)% and 1.56(3)%, respectively. The crystal structure motif in the $x=2$ is very similar to the one in the pristine compound, and thus all the crystal structure parameters can be directly compared (see Table I). The noticeable change in the trimer structure is the decrease in Cu1-O4-Cu2 bond angle. Similar to the $x=1$ compound, the Ni atoms predominantly occupy the end positions, while the middle position is mainly occupied by Cu. Table II shows the average cation-oxygen bond lengths and the distortions of all the polyhedra and the bond valence sum (BVS) for all cations calculated from the experimental distances using FULLPROF suite[9] and the BVS parameters from Ref. 12. The BVSs for the oxygen atoms (not shown in the table) are very close to 2.

IV. MAGNETIC STRUCTURE OF $x=2$ COMPOUND

The magnetic susceptibility data are presented in Fig. 6. The susceptibility of the composition with $x=1$ that does not exhibit magnetic ordering down to 1.5 K is also shown in the plot for comparison. The high-temperature part of the susceptibility ($T=75-225$ K) was fitted to $\chi(T)=C/(T-T_{\mathrm{CW}})+B$, where $C=N_A 2S(S+1)\mu_B/3k$ is the Curie constant and B is a constant background term due to the impurity phases. The fit results are shown in the inset of Fig. 6. The paramagnetic spin values per magnetic site Cu^{2+}/Ni^{2+} calculated from the refined values of the Curie constant C amounted to $S=0.92(1)$ and 0.96(2) that are in reasonable agreement with the expected average spin values per magnetic site, 0.67 and 0.83 for $x=1$ and $x=2$ compositions, respectively. The broad peak at $T_N=20$ K is associated with a transition to the magnetically ordered state. The high statistics neutron diffraction patterns were collected at the temperatures below ($T=1.5$ K) and above (25 K) the transition at T_N using neutron wavelength $\lambda=4.2$ Å. The low-temperature pattern possesses many additional magnetic Bragg peaks that prove the presence of long-range magnetic ordering. The difference pattern (1.5 K−25 K) containing purely magnetic contribution is shown in Fig. 7. The temperature scan performed in the temperature range from 1.5 to 21 K confirms that the magnetic Bragg peaks disappear above 18 K. The Bragg peaks of the difference pattern can be excellently indexed in the chemical cell of the $x=2$ compound with the propagation vector $\mathbf{k}=\left[\frac{1}{2}\frac{1}{2}0\right]$, thus proving the antiferromagnetic nature of the transition at T_N. The powder profile matching refinement (Fig. 7) shows that all the peaks are well described in the above model ($R_{wp}=8.9$, $R_{\mathrm{exp}}=6.7$, $\chi^2=1.73$, and $\chi^2_{\mathrm{Bragg}}=1.92$). The small peculiarities near $2\theta\simeq 33.15°$, 81.6°, and 69.4° are due to the slight position mismatch of the intense nuclear Bragg peaks for the two temperatures.

A. Symmetry analysis

Using the determined propagation vector, we performed the symmetry analysis according to Izyumov *et al.*[13] to derive possible magnetic configurations for both Ni ($8f$) and Cu ($4b$) magnetic sites of the space group $C12/c1$ (No. 15).

TABLE I. The structure parameters and Cu(Ni)-O interatomic distances in $Ca_3Cu_3(PO_4)_4$ ($x=0$) and $Ca_3Cu_2Ni(PO_4)_4$ ($x=1$) [space group $P12_1/a1$ (No. 14)] and $Ca_3CuNi_2(PO_4)_4$ ($x=2$) [space group $C12/c1$ (No. 15)]. The Wyckoff positions are 2*a* for Cu1, 2*b* for Ca1, and 4*e* for other atoms for the compounds with $x=0,1$ and 4*b* for Cu1, 4*e* for Ca1, and 8*f* for other atoms for the $x=2$ one. The data are refined from the powder neutron diffraction patterns measured at HRPT/SINQ with wavelength $\lambda=1.886$ Å. Bragg reliability factor R_{Bragg} for the main phase and conventional reliability factors for the whole pattern, $R_{\mathrm{wp}}, R_{\mathrm{exp}}$, and χ^2, are also given. The notation of the oxygen atoms around the Cu2-Cu1-Cu2 trimer is given in Fig. 2. The bond lengths are given in Å, the angles in deg, and the isotropic thermal displacement parameter *B* in $Å^2$. For the Cu1 and Cu2 positions, the refined occupancies Cu/Ni are given.

	$x=0$	$x=1$	$x=2$
a (Å)	17.62154(8)	17.71388(9)	17.7174(1)
b (Å)	4.90205(2)	4.88512(2)	4.82109(4)
c (Å)	8.92224(5)	8.84635(5)	17.8475(1)
γ (deg)	124.0744(3)	123.8436(3)	123.6373(5)
V ($Å^3$)	638.39	635.81	1269.22
x,y,z	0,0,0	0,0,0	$\frac{1}{2},0,0$
B (Cu1)	0.64(4)	0.74(6)	0.81(8)
Cu/Ni	1/0	0.980/0.020(15)	0.84/0.16(2)
x,y,z	0.1198(1),0.4771(3),0.9430(2)	0.1213(1),0.4717(3),0.9461(2)	0.6199(1),0.4638(4),0.4671(1)
B (Cu2)	0.39(4)	0.70(3)	0.67(4)
Cu/Ni	1/0	0.510/0.490(8)	0.08/0.92(1)
x,y,z	$\frac{1}{2},0,\frac{1}{2}$	$\frac{1}{2},0,\frac{1}{2}$	$0,0.951(1),\frac{1}{4}$
B (Ca1)	0.44(6)	0.71(8)	0.42(9)
x,y,z	0.2659(2),0.4630(6),0.7265(3)	0.2648(2),0.4648(6),0.7267(4)	0.7667(2),0.4441(8),0.3614(2)
B (Ca2)	0.80(5)	0.63(6)	0.69(7)
x,y,z	0.5934(1),0.9897(5),0.2487(3)	0.5930(2),0.9857(7),0.2480(3)	0.0933(2),0.9915(7),0.1257(2)
B (P1)	0.39(4)	0.67(4)	0.22(5)
x,y,z	0.8406(2),0.0161(5),0.2164(3)	0.8417(2),0.0175(5),0.2194(3)	0.3406(2),0.9498(7),0.1111(2)
B (P2)	0.40(4)	0.36(5)	0.35(6)
x,y,z	0.6794(2),0.9046(4),0.4240(3)	0.6798(2),0.9023(5),0.4267(3)	0.1793(2),0.0811(6),0.2121(2)
B (O1)	0.68(4)	0.68(4)	0.35(5)
x,y,z	0.0087(1),0.5519(5),0.2534(3)	0.0098(1),0.5524(5),0.2536(3)	0.5111(2),0.5214(7),0.1301(2)
B (O2)	0.68(4)	0.61(6)	0.99(6)
x,y,z	0.6006(1),0.2866(4),0.2004(3)	0.5997(2),0.2810(5),0.1927(4)	0.1017(2),0.6968(6),0.0995(2)
B (O3)	0.73(4)	0.85(4)	0.68(6)
x,y,z	0.5812(1),0.8074(4),0.0918(3)	0.5846(2),0.7987(5),0.0962(4)	0.0801(2),0.1812(6),0.0477(2)
B (O4)	0.44(4)	0.76(5)	0.45(6)
x,y,z	0.8978(2),0.8549(4),0.3861(3)	0.9014(2),0.8629(5),0.3913(4)	0.3980(2),0.1037(5),0.1972(2)
B (O5)	1.09(4)	1.62(6)	2.04(8)
x,y,z	0.8542(1),0.9282(4),0.0661(3)	0.8518(2),0.9277(5),0.0641(3)	0.3563(2),0.0482(5),0.0381(2)
B (O6)	0.66(5)	1.07(5)	1.11(6)
x,y,z	0.3574(1),0.1752(4),0.2467(3)	0.3586(2),0.1658(5),0.2433(3)	0.8542(2),0.1343(6),0.1220(2)
B (O7)	0.82(4)	1.20(6)	1.01(6)
x,y,z	0.7396(1),0.9661(5),0.1521(3)	0.7429(2),0.9709(6),0.1622(3)	0.2412(2),0.9966(6),0.0806(2)
B (O8)	0.83(4)	0.95(5)	1.43(6)
R_{Bragg} (%)	1.84	1.68	1.69
$R_{\mathrm{wp}}, R_{\mathrm{exp}}, \chi^2$	2.48, 0.92, 7.23	2.68, 1.11, 5.82	3.0, 1.57, 3.68
Cu1-O4	1.917(2)	1.918(2)	1.939(3)
Cu2-O4	2.086(4)	2.099(4)	2.045(4)
Cu1-Cu2	3.534(2)	3.556(2)	3.352(2)
Cu1-O4-Cu2	123.9(2)	124.5(2)	114.6(2)
Cu1-O3	1.970(2)	1.953(2)	1.938(2)

TABLE I. (*Continued.*)

	$x=0$	$x=1$	$x=2$
Cu2-O2	1.942(2)	1.989(2)	2.003(3)
Cu2-O7	2.175(4)	2.023(3)	2.055(5)
Cu2-O8	1.898(2)	2.121(4)	1.984(3)
Cu2-O6	2.051(3)	1.946(2)	2.060(4)

For this purpose, we used program BASIREP (Ref. 9) to obtain corresponding basis functions $\boldsymbol{\psi}_{j0}$ ($3m$-dimensional vectors) in the zeroth unit cell of all atoms of the site (j) with multiplicity m. The magnetic moments are obtained by the linear combination of the basis functions:

$$\mathbf{S}_{j0} = \sum_{\lambda,k_L} C_{\lambda,\mathbf{k}_L} \boldsymbol{\psi}_{j0}, \tag{1}$$

where $\mathbf{S}_{j0}$ is a m-dimensional column of spins on the position (j), $C_{\lambda,\mathbf{k}_L}$ are arbitrary mixing coefficients, $\mathbf{k}_L$ enumerates the arms of the propagation vector star $\{\mathbf{k}\}$, and λ runs over the basis functions that appear in the decomposition of the magnetic representation. The magnetic moments of the atoms displaced by the translation $\mathbf{t}$ are obtained by the relation

$$\mathbf{S}_j(\mathbf{t}) = \mathbf{S}_{j0} \exp(2\pi i \mathbf{k}\mathbf{t}), \tag{2}$$

where $\mathbf{t}$ is a centering translation $(\frac{1}{2}\frac{1}{2}0)+$ or chemical cell translations.

The little group G_k of propagation vector contains two elements $\{1,\bar{1}\}$. The star of propagation vector has two arms $\mathbf{k}_1=[\frac{1}{2}\frac{1}{2}0]$ and $\mathbf{k}_2=[-\frac{1}{2}\frac{1}{2}0]$ that are related by the 2_y symmetry operator. The reciprocal $\mathbf{a}^*\mathbf{b}^*$ plane showing the propagation vector star in both centered and primitive unit cells is presented in Fig. 8. There exist two one-dimensional real irreducible representations τ_1 and τ_2 with the characters (1,1) and $(1,-1)$, respectively. For completeness, we give the k vector in the settings used in the Kovalev's book.[14] Kovalev uses $B112/b$ settings for the space group 15 with the transformation matrix $\mathbf{A}=\mathbf{a}$, $\mathbf{B}=\mathbf{c}$, and $\mathbf{C}=-\mathbf{b}$, where the capital and lowercase letters are the basis vectors for $B112/b$ and standard $C12/c1$ settings. The relationship between the centered $B2/b$ cell and Kovalev's choice of primitive lattice is given by (p. 57 of Ref. 14) $\mathbf{a}=\mathbf{A}$, $\mathbf{b}=-(\mathbf{A}+\mathbf{C})/2$, and $\mathbf{c}=(-\mathbf{A}+\mathbf{C})/2$, where the lowercase letters stand for the primitive cell. Using the above matrices, we find that the k vector star in the primitive Kovalev basis reads $\{[0,0,\frac{1}{2}],[0,\frac{1}{2},0]\}$, which corresponds to the star $\mathbf{k}_4$ in the Kovalev's notations. The representation of this $\mathbf{k}_4$-vector group contains two one-dimensional irreps τ_1 and τ_2 (pp. 59 and 229 of Ref. 14) in accordance with the BASIREP calculations.

The decomposition of the axial vector representations for Cu and Ni sites reads $3\tau_2$ and $3\tau_1 \oplus 3\tau_2$, respectively. Only τ_2 appears in the decomposition for both magnetic sites, and hence we conclude that the magnetic ordering goes according to the representation τ_2. In the zeroth cell, there are two Cu atoms and four Ni atoms (centering translation excluded). Both Ni and Cu sites are split into two independent orbits as shown in Table III. The atoms on the second orbits are obtained from the first ones by applying a rotation 2_y around $(0,y,\frac{1}{4})$. Table III shows the basis functions of τ_2 that will be used below. Actually, in our case, the basis functions for both orbits and both arms of the star $\{\mathbf{k}\}$ can be chosen to be the same as the functions for the orbit 1 and the propagation vector $\mathbf{k}_1$. However, we have also constructed a special case of the basis functions for the orbit 2 shown in Table III for the purposes we explain below.

Inside of each the Ni orbits, the spins are antiparallel and have the same magnitude for the τ_2 representation. The trimers are formed by the two Ni atoms related by inversion with the Cu in the inversion center. Since the Cu atoms are in the positions $(0\ \frac{1}{2}\ 0)$ or $(0\ \frac{1}{2}\ \frac{1}{2})$, the inversion about Cu moves the Ni atom out of the zeroth cell to the neighboring cell shifted either along the x or y axis (shift along the z axis is not important). This translation reverses the Ni spin according to Eq. (2), leaving the Ni spins parallel in the trimers.

B. Magnetic structure determination

The spin components for both Cu and Ni atoms are unrestricted by symmetry giving, in general, 12 independent pa-

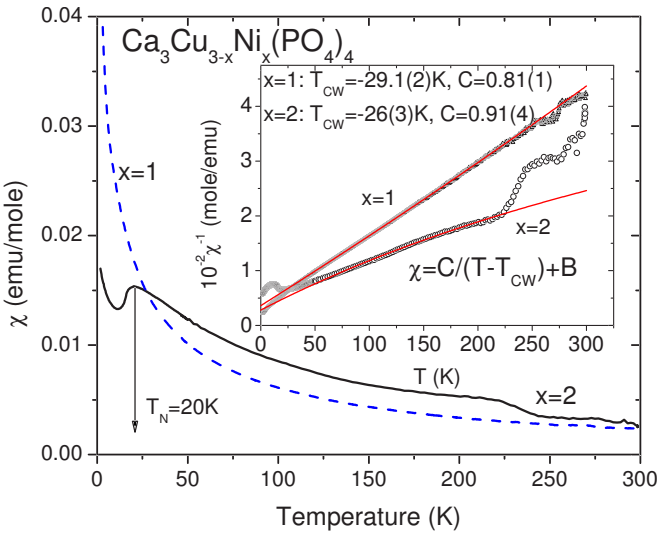

FIG. 6. (Color online) Real part of the ac magnetic susceptibility is shown as a function of temperature for the samples $Ca_3Cu_{3-x}Ni_x(PO_4)_4$ with $x=1$ and 2. The inset shows the inverse susceptibility with the least-squares fit to the Curie-Weiss law. The susceptibility is given per mole of the magnetic ions (Ni or Cu). The refined Curie-Weiss transition temperatures T_{CW} and the Curie constants C are shown in the inset.

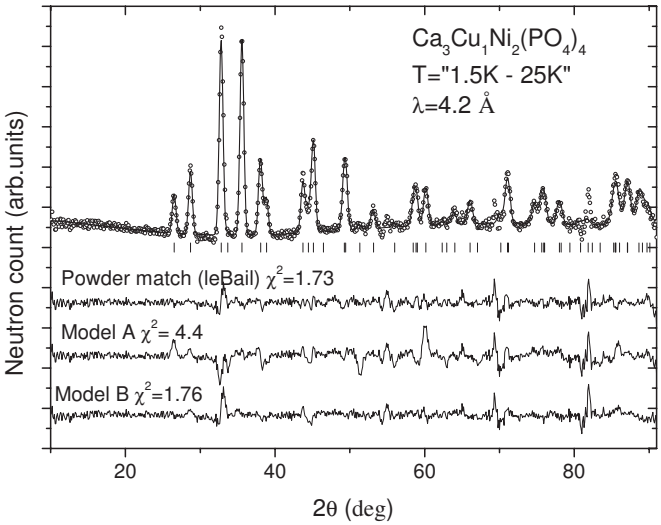

FIG. 7. The Rietveld refinement pattern and difference plot of the difference magnetic neutron diffraction pattern between 1.5 and 25 K for the sample with $Ca_3Cu_{3-x}Ni_x(PO_4)_4$ ($x=0.2$) at $T=290$ K at DMC with the wavelength $\lambda=4.2$ Å. The difference curves are shown for three different refinements: profile matching mode (the model contains only unit cell parameters and the propagation vector) and two different models. See the text for details.

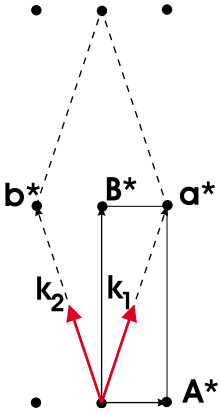

FIG. 8. (Color online) The reciprocal $\mathbf{a}^*\mathbf{b}^*$ plane showing both conventional (direct space centered $C12/c1$ setting) and primitive reciprocal cells by the dotted and solid lines, respectively. The primitive basis vectors are related to the conventional ones as $\mathbf{a}^*=\mathbf{A}^*+\mathbf{B}^*$ and $\mathbf{b}^*=-\mathbf{A}^*+\mathbf{B}^*$. The propagation vector star is shown by $\{\mathbf{k}_1,\mathbf{k}_2\}$.

rameters: one Ni spin and one Cu spin for each orbit. However, we constrain the sizes of the spins of the atoms to be equal in both orbits, because the inneratomic energies generating the atomic spin are much larger than the interatomic exchange interactions. The atom positions were fixed by the values determined from the HRPT diffraction pattern measured at 25 K with $\lambda=1.886$ Å. We performed a simulated annealing minimization[15] of the integrated intensities of the 46 magnetic Bragg peaks using FULLPROF program for this general model (A) using one arm of $\{\mathbf{k}\}$. Finally, the result of the simulated annealing search was refined using usual Rietveld refinement of the powder diffraction pattern. The best fit (model A) is shown in Fig. 7. The fit quality is not really good if we compare the $\chi^2=4.5$ with the one obtained in the powder matching fit $\chi^2=1.7$ as shown in Fig. 7. We have to conclude that there is no satisfactory solution in the model with one arm of the propagation vector star $\{\mathbf{k}\}$. However, for completeness, we present the fit results for this model in Table IV.

We have found a real solution considering both arms of the star $\{\mathbf{k}\}$, which excellently fits to the experimental data (model B in Fig. 7). At first, we considered only orbit 1 with the propagation vector $\mathbf{k}_1$, i.e., only half of the atoms, and obtained an excellent fit. Then, we have constricted the basis functions of the vector $\mathbf{k}_2$ from the ones for the vector $\mathbf{k}_1$ by the using the relation [formula (9.15) of Ref. 13]

$$\psi(\mathbf{k}_2,j') = \exp(-2\pi i \mathbf{k}_2 \mathbf{a}_p(g_2,j))\,\delta_{g_2}\hat{R}(h_{g_2})\psi(\mathbf{k}_1,j), \quad (3)$$

where g_2 is the symmetry element generating the arm $\mathbf{k}_2$, j and j' are the initial atom number and the atom number after applying g_2, $\mathbf{a}_p(g_2,j)$ is a translation returning the transformed by g_2 atom j' to the zeroth cell, $\hat{R}(h_{g_2})$ is the rotation matrix of the operator g_2, δ_{g_2} is 1 (−1) for the proper (im-

TABLE II. The average cation-oxygen bond lengths d, the rms distortion of the polyhedra, $\delta d/d$, in units 10^{-4}, and the bond valence sum (BVS) calculated from the experimental distances using FULLPROF suite (Ref. 9) and the BVS parameters from (Ref. 12). C and V are the coordination of the polyhedra and the nominal cation valence, respectively.

			$x=0$			$x=1$			$x=2$		
Atom	C	V	d (Å)	$\delta d/d$	BVS	d (Å)	$\delta d/d$	BVS	d (Å)	$\delta d/d$	BVS
Cu1	4	2	1.9450(9)	1.5	1.953(5)	1.9358(10)	0.5	2.000(5)	1.9387(13)	0.002	1.983(8)
Ni1	4	2						1.869(5)			1.853(41)
Cu2	5	2	2.0290(13)	24.3	2.013(6)	2.0336(13)	10.9	1.950(12)			1.947(41)
Ni2	5	2						1.822(12)	2.0293(16)	2.2	1.819(8)
Ca1	6	2	2.3331(9)	5.1	2.253(6)	2.3273(8)	4.4	2.286(5)	2.3361(16)	18.4	2.290(11)
Ca2	3	2	2.3714(21)	2.0	1.010(6)	2.3707(22)	6.0	1.020(6)	2.4017(25)	7.4	1.255(8)
P1	4	5	1.5384(17)	2.7	4.958(22)	1.5372(18)	1.3	4.969(23)	1.5298(23)	2.7	5.074(31)
P2	4	5	1.5343(17)	2.5	5.014(22)	1.5357(18)	4.9	5.005(24)	1.5297(23)	2.6	5.077(32)

TABLE III. Positions of the magnetic atoms in the zeroth unit cell, symmetry operators of G_k and G (space group $G=C12/c1$, propagation vector $\mathbf{k}=[\frac{1}{2}\frac{1}{2}0]$), and basis functions for irreducible representation τ_2. The Ni atom is in general position $8f$ with coordinates (0.620 65, 0.535 30, 0.967 95), and the Cu atom is in $4b$ position $(0,\frac{1}{2},0)$. The atoms of orbit 2 are generated from the respective atoms of orbit 1 by the symmetry element $(2\ 0,y,\frac{1}{4})$. The basis functions for orbit 2 are constructed using formula (3).

Atom	Equivalent position	Symmetry operator of $G;G_k$	τ_2	τ_2'	τ_2''
		Orbit 1, $\mathbf{k}_1=[\frac{1}{2}\frac{1}{2}0]$			
Ni11	x,y,z	1;1	100	010	001
Ni12	$-x+1,-y+1,-z+1$	$\bar{1};\bar{1}$	−100	0−10	00−1
Cu1	$0,\frac{1}{2},0$	1;1	100	010	001
		Orbit 2 $(2\ 0,y,\frac{1}{4})$, $\mathbf{k}_2=[-\frac{1}{2}\frac{1}{2}0]$			
Ni21	$-x+1,y,-z+\frac{3}{4}$	$2\ 0,y,\frac{1}{4};1$	100	0−10	001
Ni22	$x-1,-y+1,z-\frac{1}{2}$	$c\ x,0,z;-1$	−100	010	00−1
Cu2	$0,\frac{1}{2},\frac{1}{2}$	$2\ 0,y,\frac{1}{4};1$	−100	010	00−1

proper) rotation. The basis functions obtained this way are listed in Table III. Using these basis functions and considering only orbit 2 with the same mixing coefficients $C_{\lambda,\mathbf{k}_2}$ of formula (1) as for the orbit 1, we get identical Bragg peak intensities. Thus, the set of the structure factors is essentially the same for both orbits provided that the basis functions are related by transformation (3) and the propagation vectors by the matrix $\hat{R}(h_{g_2})$. We note that it cannot be a general assertion valid for arbitrary space group since a crystallographic site can split into the k star orbits containing different number of atoms. Transformation (3) moves the atoms from orbit 1 to orbit 2 and rotates the Cu spin by π around the y axis, while for the Ni atoms, it reflects the spin about the ac plane.

In our case, the equivalence of the structure factors for orbit 1, $\mathbf{k}_1$, and orbit 2, $\mathbf{k}_2$, with the basis functions listed in Table III can be easily seen if we consider the primitive unit cell. The primitive basis vectors are related to the ones of the C-centered lattice as $\mathbf{a}=(\mathbf{A}+\mathbf{B})/2$, $\mathbf{b}=(-\mathbf{A}+\mathbf{B})/2$, and $\mathbf{c}=\mathbf{C}$, where the lowercase letters stand for the primitive basis. In the zeroth primitive unit cell, the spins of Cu and Ni on each orbit are parallel and the spins on different orbits are related by a π rotation about $\mathbf{B}$. The propagation vectors are $\mathbf{k}_1=[\frac{1}{2},0,0]$ and $\mathbf{k}_2=[0,\frac{1}{2},0]$ as shown in Fig. 8. The origin of the space group can be shifted by $\frac{1}{2}$ along the $\mathbf{c}$ axis. Since the structure factor is calculated only for the atoms on one orbit, we shift orbit 2 by $(0,0,-\frac{1}{2})$, so that the Cu atom stays in the same position $(\frac{1}{2},\frac{1}{2},0)$ for both orbits. The Ni11 and Ni12 are in (x,y,z) and $(\bar{1}-x,1-y,1-z)$; the Ni21 and Ni22 are in $(1-y,1-x,z)$ and $(y,x,1-z)$. The magnetic structure factor is $\mathbf{F}(\mathbf{H})\propto\Sigma_j\mathbf{M}_{\perp j}\exp(\mathbf{H}\mathbf{r}_j)$ for the scattering vector $\mathbf{H}=\mathbf{h}+\mathbf{k}$, where $\mathbf{h}$ is a reciprocal lattice vector of the crystal structure, $\mathbf{M}_{\perp j}=\mathbf{H}\times[\mathbf{M}_j\times\mathbf{H}]/H^2$, and the sum runs over Cu and two Ni atoms at the positions r_j with the magnetic moments $\mathbf{M}_j$. The phase factor for Cu is the same for both orbits, the phase factors for Ni11 and Ni22 and for Ni12 and Ni21 will be the same if we choose the reflections $\mathbf{H}_1=(h,k,l)+\mathbf{k}_1$ and $\mathbf{H}_2=(k,h,-l)+\mathbf{k}_2$ for orbits 1 and 2, respectively. The reciprocal vectors $\mathbf{H}_1$ and $\mathbf{H}_2$ are related by π rotation about the $\mathbf{B}^*$ axis (Fig. 8) and hence have the same length and give the Bragg peaks at the same 2θ position in the powder diffraction pattern. Since the spins on two orbits are also related by a π rotation about the $\mathbf{B}$ axis, which is collinear to $\mathbf{B}^*$, the vectors $\mathbf{M}_{\perp j}$ are also related by a π rotation about the $\mathbf{B}$ axis. Hence, the intensity $I\propto|\mathbf{F}|^2$ will be

TABLE IV. Magnetic model parameters for $Ca_3Cu_{3-x}Ni_x(PO_4)_4$ ($x=2$) refined from the diffraction data shown in Fig. 7. The numeration of the atoms is the same as in Table III. M is the size of the magnetic moment; ϕ and θ are spherical angles with c (azimuth) and b (zenith) axes, respectively. The graphical illustration of the spherical angles is given in Fig. 9. The error bars are given only for the independently refined parameters. Model A does not fit the data but is given for completeness. See the text for details. In models B and C, $\phi_{Ni21}=\phi_{Ni11}$, $\theta_{Ni21}=\pi-\theta_{Ni11}$, $\phi_{Cu2}=\phi_{Cu1}+\pi$, and $\theta_{Cu2}=\theta_{Cu1}$. In model C, the spins of Ni and Cu are constrained to be (anti)parallel in the trimers.

	Model A			Model B			Model C		
	M (μ_B)	ϕ	θ	M (μ_B)	ϕ	θ	M (μ_B)	ϕ	θ
Ni11	1.760(2)	104.3(1.2)	78.4(1.5)	1.892(9)	176.1(8)	83.98(45)	1.883(8)	175.9(9)	83.4(4)
Cu1	1.196(4)	21.2(4.4)	47.5(3.1)	0.62(2)	153.5(3.7)	103.3(2.9)	0.57(1)	175.9	96.6
Ni21	1.760	12.4(1.7)	69.9(1.3)	1.892	176.1	96.02	1.883	175.9	96.6
Cu2	1.196	26.9(4.3)	127.7(4.1)	0.62	333.5	103.3	0.565	355.9	96.6
$R_{wp},R_{exp},\chi^2,\chi_B^2$	14.1, 6.7, 4.4, 5.1			8.9, 6.7, 1.76, 1.93			9.2, 6.7, 1.86, 2.05		

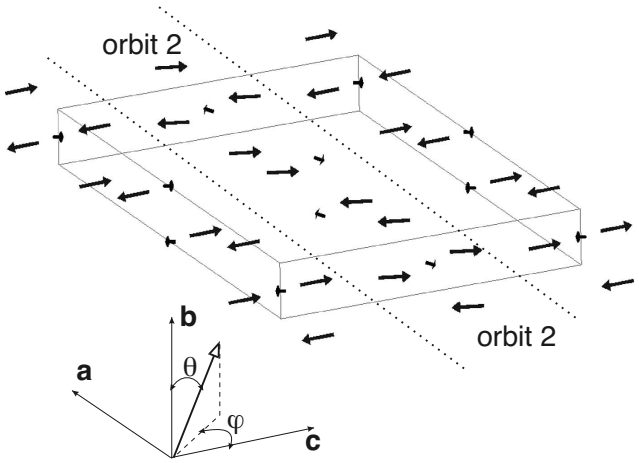

FIG. 9. The zeroth unit cell of $Ca_3Cu_{3-x}Ni_x(PO_4)_4$ ($x=2$) showing the configuration of the Ni and Cu spins. Some of the Ni spins from the neighboring cells are shown for better visibility of the trimers. The unit cell constants at $T=25$ K are $a=17.724$ Å, $b=4.815$ Å, $c=17.836$ Å, and $\beta=123.756°$ ($C2/c$ space group). The spins in the middle of the cell along the c direction between the dotted lines belong to orbit 2 (Cu2, Ni21, and Ni22 spins) and have propagation vector $\mathbf{k}_2=\left[-\frac{1}{2}\frac{1}{2}0\right]$, and the other spins belong to orbit 1 (Cu1, Ni11, and Ni12 spins) and have propagation vector $\mathbf{k}_1=\left[\frac{1}{2}\frac{1}{2}0\right]$. The structure corresponds to model B shown in Table IV. The crystal axes and the spherical angles used in Table IV are also shown.

the same for the Bragg peaks located at H_1 and H_2 for orbits 1 and 2, respectively, and the powder diffraction patterns generated by orbits 1 and 2 will be identical.

The two orbits do not interfere with each other because of different propagation vectors. Hence, using all the atoms, we naturally get the same fit quality with $\sqrt{2}$ smaller mixing coefficients. The results of the fit are shown in Fig. 7 (marked as model B). This model contains only six refinable parameters and gives the same fit quality as the powder matching refinement, implying that the fit cannot be better for the given propagation vector $\mathbf{k}$. The imperfection of the fits near $2\theta=33.2°$ and 54.7° seen in both the powder match and the model B difference curves is apparently due to a "nonideal" subtraction (1.5 K−25 K) of the large nuclear peaks (002) and (110) at these angular positions. Another explanation could be the presence of weak ferromagnetism, but it is beyond the accuracy of our experimental data.

In this model, there is no mixing of the basis functions of $\mathbf{k}_1$ and $\mathbf{k}_2$ on the same orbit, and thus it gives constant moment configurations for any direction of the spins. The assumption of having the same mixing coefficient for the atoms on the different orbits and belonging to the different arms is not dictated by symmetry, because the coefficients $C_{\lambda,\mathbf{k}_L}$ in formula (1) are independent quantities for $\mathbf{k}_1$ and $\mathbf{k}_2$. However, in our particular case, this assumption gives an excellent fit and good spin values as shown in Table IV (model B).

The best fit magnetic configuration is shown in Fig. 9. The figure shows 1/4 part of the magnetic unit cell. The whole magnetic cell contains 48 magnetic atoms. The mutual orientations of the spins in the trimers are different for the trimers on orbits 1 and 2. On the first orbit, the Ni and Cu spins are close to antiparallel configuration, whereas on the second orbit, they are close to a ferromagnetic coupling. Intuitively, one would expect to have the same spin orientation in all the trimers, because the intratrimer interactions should be the strongest ones. To make the trimers identical, one should constrain the Ni spin to be parallel to the c axis and the Cu spin to be in the plane perpendicular to the c axis. For this configuration, Cu and Ni spins are perpendicular for both trimers. However, this constrained model gives a very bad goodness of fit, $\chi^2=8.67$, and has to be rejected. Since the spins in the trimers are close to a parallel orientation, we also tried to constrain them to be parallel (model C in Table IV). This constrained model gives only slightly worse χ^2 than the general case. The model contains only four adjustable parameters: two spin values and two angles that are not bad for describing the intensities of 46 magnetic Bragg peaks. The spins are aligned roughly along the c axis with very small canting as shown in Table IV. We note that the sublattices of the trimers corresponding to the different arms of the star $\{\mathbf{k}\}$ do not interfere with each other and the magnetic configuration, in which all the spins in the trimers on the same orbit are reversed, will give the same Bragg peak intensities. Thus, we can have two types of domains with the reversed mutual orientation trimer spins on orbits 1 and 2.

From the above proof of the equivalence of the structure factors for orbit 1 with $\mathbf{k}_1$ and orbit 2 with $\mathbf{k}_2$, one can see that the model with the atoms from orbit 2 and with the propagation vector $\mathbf{k}_1$ ("orbit2+k1") is not an allowed equivalent solution. We tried to find a solution by fitting the data to the orbit2+k1 model, but the best solution has much worse $\chi^2_{\text{Bragg}}=5.1$ similar to model A. The reason is the difference of the phase factors for Ni in the structure factor $\mathbf{F}(\mathbf{H})$. For example, the phase factor for Ni atoms in the structure factor for the $\left(\frac{1}{2},0,0\right)$ peak is proportional to $\sin(\pi x)$ for orbit 1 but to $\sin(\pi y)$ for orbit 2 (we use the primitive cell settings). It is clear that the x and y coordinates have no any symmetry relation with the spin value $M_\perp$. Thus, the intensity of the $\left(\frac{1}{2},0,0\right)$ peak for orbit 2 and propagation vector $\mathbf{k}_1$ will depend also on the particular value of y but not only on $M_\perp$.

V. DISCUSSION AND CONCLUSIONS

The Ni^{2+} ion always likes to occupy the end positions of the trimers. The valence of Ni if it would occupy the position Cu1 in the center of the trimer has reasonable value according to BVS calculations (Table II) and so in this respect, Ni could occupy the middle position. Apparently, the total crystal energy is minimized for the Cu being in the middle position. It is interesting to note that the distorted square pyramids $Cu2O_5$ and the distorted square planes $Cu1O_4$ become much less distorted when going from $x=0$ to $x=2$ compositions (Table II). We note that the decrease in the distortion of the polyhedron around Cu2 site in the $x=2$ compound, where it is occupied solely by Ni ions, is in accordance with the fact that Ni^{2+} ($3d^8$) is non-Jahn-Teller active ion.

The trimers in the $x=1$ composition can be of three types: Cu-Cu-Cu, Cu-Cu-Ni, and Ni-Cu-Ni, with the statistical populations of 25%/50%/25%, respectively. From the diffraction data alone, we cannot determine these populations, but from the analysis of the magnetic excitations in the trimers,[6] the real populations were determined to be 36%/28%/36%, implying that the nonsymmetric Cu-Cu-Ni trimer is significantly less populated with respect to the "ideal" statistical value. The fact that Ni atom does not occupy the middle position has precluded from the realization of the Bose-Einstein condensation in this trimer system; however, it might be worth trying to make the Ni substitution in the similar compounds $A_3Cu_3(PO_4)_4$ ($A=$Pb, Sr).

The antiferromagnetic ordering, which we have found in the $x=2$ sample, occurs at much higher temperature ($T_N=20$ K) than in the parent $x=0$ compound ($T_N=0.9$ K). The higher T_N might be due to the increase in the dipole interaction strength: Ni ion has two times larger spin value, and the intertrimer distances between the Cu2 sites along the a axis and z axis are decreased from 4.8 to 4.5 Å and from 6.5 to 6.4 Å, respectively. In addition, the superexchange (SE) coupling is expected to be larger in the $x=2$ compound. The SE interaction between the (1D) trimer chains along the b axis (as explained in Sec. III) is mediated by the Cu2-O-P2-O-Cu2 path. The completely closed P^{5+} $2p$ shells provide SE path that can be both anti- and ferromagnetic. The average Cu-O-P bond angle is increased from 126.3° to 128.5°, implying that the antiferromagnetic SE via Ni($3d$)-O($2p$) orbitals can be larger in the $x=2$ compound.

The antiferromagnetic structure can be well described only using both arms of the propagation vector star. It is quite unusual that the two-k case can be revealed from the unpolarized powder diffraction data analysis. However, the two-k solution excellently describes the data with minimal number of the refined parameters. For further verification of our magnetic structure model, the single crystal diffraction experiments might be useful. According to our model, the spin orientation in the Ni-Cu-Ni trimers can be both anti- and ferromagnetic. The chains of the trimers running along the a axis are of two types: one consisting of the antiferromagnetic (AFM) trimers and another one with the ferromagnetic (FM) trimers. The Ni^{2+} ordered magnetic moment of 1.9 μ_B is close to the saturated value, whereas the Cu^{2+} moment of 0.6 μ_B is substantially smaller than the spin-only value. This might be due to frustration of the Cu moment, i.e., some trimers in the AFM trimer chain have Cu spins aligned ferromagnetically with Ni ones and vice versa for the FM chains.

In conclusion, we have successfully synthesized and studied the crystal and magnetic structures of the mixed spin trimers $Ca_3Cu_{3-x}Ni_x(PO_4)_4$ ($x=0,1,2$) by means of neutron diffraction in the temperature range 1.5–290 K. Our work forms an important ground for the inelastic neutron scattering study of the dynamic magnetic properties of this system.

ACKNOWLEDGMENTS

This study was performed at Swiss neutron spallation SINQ and Swiss light source SLS of Paul Scherrer Institute PSI (Villigen, PSI). We thank L. Keller for the help in neutron diffraction measurements and P. Fischer, O. Zaharko, and Zoso L. Davies for the discussions. Financial support by the NCCR MaNEP project is gratefully acknowledged.

[1] A. A. Belik, A. P. Malakhov, B. I. Lazoryak, and S. S. Khasanov, J. Solid State Chem. **163**, 121 (2002).
[2] M. Matsuda, K. Kakurai, A. A. Belik, M. Azuma, M. Takano, and M. Fujita, Phys. Rev. B **71**, 144411 (2005).
[3] M. Drillon, M. Belaiche, P. Legoll, J. Aride, A. Boukhari, and A. Moqine, J. Magn. Magn. Mater. **128**, 83 (1993).
[4] A. A. Belik, A. Matsuo, M. Azuma, K. Kindo, and M. Takano, J. Solid State Chem. **178**, 709 (2005).
[5] C. Ruegg, N. Cavadini, A. Furrer, H. U. Gudel, K. Kramer, H. Mutka, A. K. Habicht, P. Vorderwisch, and A. Wildes, Nature (London) **423**, 62 (2003).
[6] A. Podlesnyak, V. Pomjakushin, E. Pomjakushina, K. Conder, and A. Furrer, Phys. Rev. B **76**, 064420 (2007).
[7] P. Fischer *et al.*, Physica B **276-278**, 146 (2000).
[8] P. Fischer, L. Keller, J. Schefer, and J. Kohlbrecher, Neutron News **11**, 19 (2000).
[9] J. Rodriguez-Carvajal, Physica B **192**, 55 (1993).
[10] B. I. Lazoryak, N. Khan, V. A. Morozov, A. A. Belik, and S. S. Khasanov, J. Solid State Chem. **145**, 345 (1999).
[11] V. Favre-Nicolin and R. Cerny, J. Appl. Crystallogr. **35**, 734 (2002).
[12] I. D. Brown and D. Altermatt, Acta Crystallogr., Sect. B: Struct. Sci. **41**, 244 (1985).
[13] Y. A. Izyumov, V. E. Naish, and R. P. Ozerov, *Neutron Diffraction of Magnetic Materials* (Consultants Bureau, New York, 1991).
[14] O. V. Kovalev, *Representations of the Crystallographic Space Groups: Irreducible Representations, Induced Representations, and Corepresentations*, 2nd ed. (Gordon and Breach, New York, 1993).
[15] S. Kirkpatrick, C. D. Gelatt, and M. P. Vecchi, Science **220**, 671 (1983).